Characteristics and Statistics of Tropical Cyclone Tornadoes and Warning Skill

WALTER MCGAVRAN*

National Weather Center Research Experiences for Undergraduates Program
Norman, Oklahoma,
Loyola University Chicago
Chicago, Illinois, USA

BENJAMIN A. SCHENKEL

Cooperative Institute for Severe and High-Impact Weather Research and Operations
Norman, Oklahoma, USA
NOAA/OAR National Severe Storms Laboratory
Norman, Oklahoma, USA
School of Meteorology, University of Oklahoma
Norman, OK

THEA N. SANDMÆL

Cooperative Institute for Severe and High-Impact Weather Research and Operations
Norman, Oklahoma, USA
NOAA/OAR National Severe Storms Laboratory
Norman, Oklahoma, USA

KRISTIN M. CALHOUN

NOAA/OAR National Severe Storms Laboratory
Norman, Oklahoma, USA

A. ADDISON ALFORD

NOAA/OAR National Severe Storms Laboratory
Norman, Oklahoma, USA

ABSTRACT

Landfalling tropical cyclones (TCs) often spawn tornadoes, which yield conflicting call-to-actions between tornado warnings and those issued for other hazards (e.g., flash flooding). There have only been a limited number of TC case studies examining tornado warning forecast skill within TC environments, often yielding differing results. Hence, this study conducts a climatological analysis of tornado warning skill within TCs from 2011–2021, using observed TC and tornado data in conjunction with single-radar data quantifying low-level rotation and convergence. Tornado warning skill was lower for TC tornadoes than values of non-TC tornadoes cited in prior work. Warning skill was generally insensitive to parameters like distance from the TC center, time of day, and TC intensity. However, despite the low number of tornadoes far from the TC center (i.e., $\geq$600 km), warning issuance was still very high, resulting in poor forecasting performance. Additionally, tornadoes that occurred after local sunset were forecast with greater skill than had previously been demonstrated, with tornado detection comparable to daytime rates. Probability of detection was substantially increased with increasing tornado damage rating. To explore forecasting thresholds that could increase skill, low-level azimuthal (i.e., quantifying low-level rotation) and divergent shear (i.e., quantifying low-level convergence) were examined which showed that warned tornadic supercells typically had strong values compared to both non-warned tornadic supercells and warned nontornadic supercells. Together, this work provides a groundwork for potentially improving tornado forecast skill in landfalling TCs.

1. Introduction

Landfalling tropical cyclones (TCs) are frequently accompanied by tornadoes (comprising ∼6% of all tornadoes in the US), which complicates emergency preparedness and response efforts for other associated hazards (e.g., flash flooding; Edwards 2012; Blake and Zelinsky 2018; Stewart and Berg 2019). Some fundamental attributes of these tornadoes are well detailed, specifically ∼93% of TC tornadoes have damage ratings of EF/F0–1 on the enhanced Fujita (EF) or Fujita (F) scales, as compared to ∼90% of non-TC tornadoes (Edwards 2010; Edwards et al. 2012). The majority (88%) of TC tornadoes are generated by supercells (Edwards et al. 2012). While neither the appearance nor the general dynamics are distinctive from those in the Great Plains region, these supercells are often low-topped and are characterized by shallower updrafts, more compact mesocyclone diameters, weaker amplitudes, and shorter lifespans (McCaul and Weisman 1996; Suzuki et al. 2000; Edwards et al. 2012). Tornado distribution in TCs falls predominantly in the northeast (pole-relative) or right-front (TC motion-relative) quadrant in the outer rainbands during local daylight hours (Schultz and Cecil 2009; Edwards 2012). However, a larger concentration of more damaging tornadoes occurs overnight (McCaul 1991; Schultz and Cecil 2009; Edwards 2012).

Similar to midlatitude supercellular tornadoes, TC supercells are heavily influenced by their specific environments. As such, operational forecasters use a variety of environmental indicators to forecast tornado risk. On the synoptic scale, TCs that encounter ambient westerly winds tend to experience enhanced vertical wind profiles favorable to supercell development, typically yielding larger numbers of tornadoes that are concentrated on the eastern half of the TC (Molinari and Vollaro 2010; Edwards 2012; Schenkel et al. 2020). On the TC scale, convective available potential energy (CAPE) and vertical wind shear are favorable for supercell development offshore, suggesting the TC-associated waterspouts could be common (Edwards 2012). However, some embedded supercells strengthen during landfall as they encounter greater friction over land compared to the ocean (Gentry 1983; Baker et al. 2009). Factors supporting inland supercell development, including those forming before the landfall of the TC center, are better studied than those developed over water (Edwards 2012). Despite their frequent occurrence, inner-band TC tornadoes and associated discrete supercells are less likely to occur inward toward the eyewall of strong cyclones for multiple reasons. Both the TC winds and convective-scale vertical wind shear tend to increase towards the TC center (Franklin et al. 2003). In conjunction with this, the convective mode near the storm center favors non-supercellular structure, with continuous banding and coverage of non-convective rain shields (Edwards 2012). Also, much like with midlatitude supercell formation, CAPE remains important to pair with helicity for TC tornadogenesis. While helicity increases towards the TC center, CAPE typically declines as denser rainbands and deep-layer cloud cover obscure diurnal heating, limiting buoyancy (Bogner et al. 2000; Molinari et al. 2012).

Even with all these well-established environmental conditions needed for tornadogenesis, forecasters still encounter difficulty accurately predicting TC tornadoes using techniques honed for non-TC environments. As a result, warning skill tends to be lower when compared with forecasting those in the Great Plains (Martinaitis 2017; Nowotarski et al. 2021). Forecasting practices can vary from office to office depending on their familiarity with tornadic storms *and* TCs, while tornadic and non-tornadic cells may show similar lightning and radar characteristics in TCs (McCaul et al. 2004; Schneider and Sharp 2007; Edwards 2012). To quantify this forecast skill, several different statistics are used, including probability of detection (POD), false alarm ratio (FAR), and critical success index (CSI; Brooks 2004; Brooks and Correia Jr. 2018). POD is generally defined in two ways: 1) the ratio of the number of forecast tornadoes to the total number of observed tornadoes (POD_1):

$$POD_1 = \frac{a}{a+c}, \tag{1}$$

where a is number of forecast tornadoes and c is the number of non-forecast observed tornadoes; or 2) the ratio of the total percentage of events warned (PEW), which is defined as the mean percentage of a tornado track which is warned:

$$POD_s = \frac{1}{N}\sum_{i=1}^{N} PEW_i, \tag{2}$$

where PEW_i is the percentage of the event warned for the ith tornado (Brooks 2004; Brooks and Correia Jr. 2018). Our study will employ the former of the two metrics for simplicity purposes as opposed to using a cell-based analysis (Nowotarski et al. 2021). While probability of detection could easily be increased by the simple issuance of more warnings, doing so would increase FAR, which is defined as the ratio of the number of forecasts without a confirmed tornado to the total number of forecasts:

$$FAR = \frac{b}{a+b}, \tag{3}$$

where b is the total number of incorrect forecasts (Brooks 2004). Additionally, CSI can be used as a tuning measure for forecasters when evaluating whether to scale up or down warning frequency, though the statistic gives no

*Corresponding author address: Walter McGavran, Loyola University Chicago, 6317 N. Broadway, Chicago, IL 60660
E-mail: wmcgavran@luc.edu

new verification information on its own. CSI can be expressed as a function of both POD and FAR:

$$CSI = \frac{1}{\frac{1}{1-FAR} + \frac{1}{POD} - 1} = \frac{a}{a+b+c}, \quad (4)$$

Hence, CSI is sensitive to changes in both parameters (Brooks 2004; Gerapetritis and Pelissier 2004). Changes in POD and FAR impact CSI equally only when the magnitude of their respective slopes are equal:

$$\left| \frac{\partial CSI}{\partial POD} \right| = \left| \frac{\partial CSI}{\partial FAR} \right|$$

which results in

$$POD = 1 - FAR. \quad (5)$$

When POD is greater than 1−FAR, changes in FAR have a greater influence on CSI than changes in POD, and vice versa (Gerapetritis and Pelissier 2004).

Because of the ubiquity of these statistics, it is useful to apply them to TC tornadoes. Indeed, it has been shown that FAR is higher for TC tornadoes than their Great Plains counterparts (Martinaitis 2017; Nowotarski et al. 2021). However, large-sample climatologies of warning statistics have not been performed with prior work, instead, examining select hurricane case studies. One notable TC to have been studied was Hurricane Harvey (2017), which produced 52 tornadoes over a record seven-day period spanning from the coast of Texas to Middle Tennessee (Nowotarski et al. 2021). Both the environmental and radar analyses performed were cell-based to prevent biasing the sample towards longer-lived cells, while the warning polygon distribution was subjectively limited to within 800 km of the center of Harvey. Tornadic and nontornadic cells associated with tornado warnings were differentiated from one another (Nowotarski et al. 2021). Warning skill and various radar attributes, notably single-radar rotational velocity (V_{rot}), were tested against previously established forecasting thresholds from Martinaitis (2017). Indeed, many of the fundamental spatial attributes of Harvey tornadoes were similar to those in the historical TCTOR database: the majority of tornadoes occurred in the northeast quadrant within a range of 100–500 km from the TC center. Temporally, Harvey was notable for its relative abundance (38.5%) of nighttime tornadoes, as compared to 29.3% in the TCTOR database (Nowotarski et al. 2021; Edwards 2012). The FAR and POD_1 for tornadoes in Harvey were found to be higher (0.84 and 0.64 respectively) than for non-TC tornadoes (0.70 and 0.53 respectively) from the previous five years (2012–16), while the CSI was found to be lower (0.16 vs 0.24; Brooks and Correia Jr. 2018; Nowotarski et al. 2021). POD experienced fluctuations as a function of distance from the TC center, while FAR steadily increased with increasing distance outwards of 200 km from the center of Harvey. Warning skill decreased notably during the night as a result of a spike in FAR. Distance from the nearest radar also revealed an inverse relationship between forecasting skill and distance. Analysis of radar data revealed that the V_{rot} was greater at all radar tilt angles for tornadic cells than nontornadic cells. However, V_{rot} decreased as a function of cell distance from the nearest radar, most likely leading to the decrease in forecasting skill with radar distance.

Building upon this prior work, the goal of the present study is to examine warning skill and radar characteristics of TC tornadoes for a large sample of TCs from 2011–2021. Specifically, the parameters of TC intensity, distance from the TC center, time relative to sunset, and damage rating will be examined in conjunction with warning skill. The radar-derived attributes azimuthal shear (AzShear; i.e., the azimuthal derivative of radial velocity quantifying rotation) and divergent shear (DivShear; i.e., the radial derivative of radial velocity quantifying divergence), which are measures of low-level rotation and divergence of the parent mesocyclones, respectively, will also be used to compare between warned tornadoes, missed tornadoes, and non-tornadic cells that were warned.

2. Data and Methods

a. TC Data

TC track and intensity (i.e., 1-min maximum 10-min wind speed) data from 2011–2021 are obtained from the National Hurricane Center HURricane DATa 2nd generation data (HURDAT2; Landsea and Franklin 2013). Our analysis uses data from the 43 TCs that each spawned $\geq$1 tornado during the period of study, defined along 6-hr reporting intervals.

b. Tornado Data

The track and damage rating data for 557 tornadoes from 2011–2021 associated with the 43 TCs listed above are obtained from the Storm Prediction Center (SPC) TC Tornado (TCTOR) database (Edwards and Mosier 2022). The data were subjectively reviewed to confirm the association of the tornado and its parent supercell with the TC. The TC-relative location of each tornado was computed using HURDAT2 data. Tornadoes may be under-sampled because of deficiencies in observations and identifying damage, which is especially challenging in a landfalling TC. Hence, this contributes to the higher false alarm ratios in TCs compared to non-TCs (Edwards et al. 2012; Nowotarski et al. 2021).

c. Nontornadic Data

Locations of strongly rotating cells were subjectively identified using 0.5°-tilt reflectivity and radial velocity, within radar scans containing $\geq$1 tornadic cell for selected landfalling TCs from 2017–2018 (Sandmæl et al.

2023). The grid point containing the maximum AzShear within a 10-km radius of the subjectively identified cell was assigned as the location for the nontornadic cell location within a radar scan. These non-tornadic cells will be used for comparison with the radar characteristics of cells where warnings were accurately and inaccurately issued.

d. Warning Data

Warning polygon vertices, centroids, and start and end times issued by National Weather Service (NWS) forecast offices as verified by the IEM archive (IEM 2020). Warnings defined as being associated with the TC were those within 1,100 km of the TC center. This is the distance at which both false alarm distributions reach a local minimum and the approximate greatest distance of tornadoes from the TC center. Tornado data from the SPC were interpolated to one-minute intervals for confirmation of overlap with individual polygons to identify "hits". The remaining warnings were considered false alarms and were collocated with the nontornadic data to aggregate radar statistics.

e. Radar Data

Both the AzShear and DivShear data, representing low-level mesocyclone rotation and convergence respectively, are computed using a 0.5°-tilt from the single-radar Next Generation Weather Radar (NEXRAD) Level 2 data (NOAA National Weather Service Operations Center 1991). Data consists of the grid point maximum AzShear and minimum DivShear recorded for both the closest radar scan to the start of the tornado and for each nontornadic cell (Mahalik et al. 2019). The location within the radar data of each cell is defined as the maximum AzShear within a 10-km distance from the tornadic or nontornadic cell. The maximum AzShear and minimum DivShear are computed within a 2.5-km distance of the radar-identified location.

3. Results

a. TC Intensity-and-Distance-Relative Variability

Data consisting of all observed tornadoes (i.e., both TC and non-TC) in the United States from 2012–2016 showed a POD of 53.0%, a FAR of 70.0%, and a CSI of 24.0% (Brooks and Correia Jr. 2018; Nowotarski et al. 2021). The sample statistics from this study were 62.5%, 87.3%, and 11.8%, which are considerably lower than non-TC cases (Martinaitis 2017; Nowotarski et al. 2021). A comparison of tornado warning skill and distribution stratified by TC intensity (Fig.1) shows that, regardless of TC intensity, warning skill, as demonstrated by CSI, remains relatively constant and in line with that of the total data, although tropical storms have comparatively slightly lower skill. This is despite tropical storms generating ∼50% of all TC tornadoes and associated warnings, which supports previous work showing that most tornadoes occur after TC landfall and that TCs spend most of their post-landfall lifespan at tropical storm intensity or weaker (Kaplan and DeMaria 1995; Schultz and Cecil 2009). The lower sample size for tornadoes associated with strong hurricanes may be a result of the greater difficulty confirming tornado occurrence, particularly near the coastline, during strong TCs where tornado damage is challenging to distinguish from the TC (Edwards et al. 2012; Edwards and Mosier 2022).

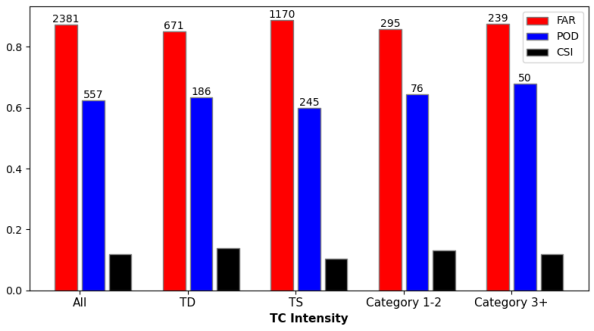

FIG. 1: Bar plot of FAR, POD, and CSI of TC tornadoes from 2011–2021 as stratified by TC intensity category. The annotation above each bar represents the number of false alarms or tornadoes in each bin. TD and TS mean tropical depression and tropical storm while the numbered categories indicate the Saffir-Simpson intensity category of the TC.

Analysis of the variability in cyclone-relative tornado warning skill (Fig. 2) shows only small differences, especially close to the TC center. Approximately 50% of all tornadoes and warnings occurred 200–400 km from the TC center (McCaul 1991; Schultz and Cecil 2009). In the 200–400 km range, POD showed a 0.3% decrease, while FAR showed a 0.5% increase in comparison, however, CSI only decreased to 11.4% for tornadoes in this area versus 11.8% for all tornadoes. Overall, for ranges with at least 100 spawned tornadoes (i.e., large sample sizes), POD remained relatively constant, though FAR experienced some variability. This is in contrast with previous case work on Harvey (2017), which demonstrated fluctuation in POD as a function of distance (Nowotarski et al. 2021). In contrast to tornadoes near the TC, those tornadoes that remain far from the TC center ($>$ 800 km) are not forecast with nearly as much precision. While only 8 tornadoes were confirmed at that distance from 2011-2021, 148 false alarm warnings were issued by WFOs resulting in a FAR of 96.7% and a CSI of 3.2%.

The variability of tornado warning skill as a function of distance from the TC center and TC intensity is shown in Fig. 3. Here, warning skill varies at different distances

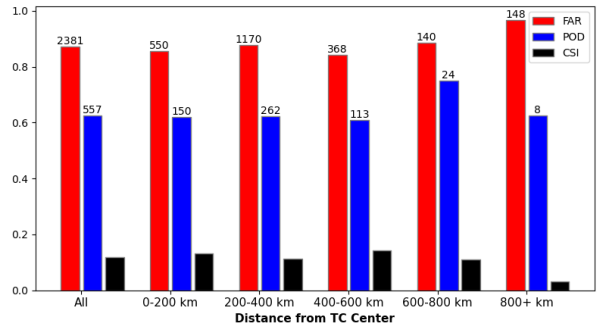

FIG. 2: As in Fig. 1, but stratified by distance from the TC center (km).

depending on the strength of the respective TC. In Fig. 2, warning skill, as demonstrated by CSI, was highest for tornadoes 400–600 km away from the TC center. When broken down by intensity, the same patterns largely hold, with the notable exception being for those associated with strong hurricanes. FAR for strong hurricanes is increased at all distances, often paired with low POD and/or small sample sizes. Juxtaposing this, FAR remains flat for tornadoes close to the center of TCs, except for strong hurricanes, while POD increases with TC intensity up until Category 1–2 hurricanes followed by a sharp drop for Category 3–5 hurricanes. For ranges beyond 600 km, sample sizes are too small when subsetting by TC intensity to make conclusive statements about the forecasting skill of TC tornadoes.

b. Variability with time of day and damage rating

The variability of warning skill relative to local sunset is investigated next (Fig. 4). The largest temporal concentration of tornadoes occurs within 6–0 hours before local sunset. Specifically, 38% of all tornadoes occur here, yet only 37% of false alarms correspond. POD is also the highest during this time frame (64.5%), and is higher than that demonstrated for all tornadoes (62.5%), while FAR (86.5%) is lower than that demonstrated for all tornadoes (87.3%). This corresponds to a CSI of 12.6%, a warning skill that surpasses that of the total TC tornado population. All of this is in agreement with previous literature and historical records (Edwards 2012).

However, the demonstrated constant warning skill after local sunset time contradicts previous individual case studies and historical records which showed or suggested lower warning skill at night (Nowotarski et al. 2021; Edwards et al. 2012). Indeed, the late-evening warning skill outperforms the morning warning skill. One possible reason for this discrepancy with historical records is a change in radar scanning strategy in 2011, Supplemental Adaptive Intra-Volume Low-Level scan (SAILS); this process

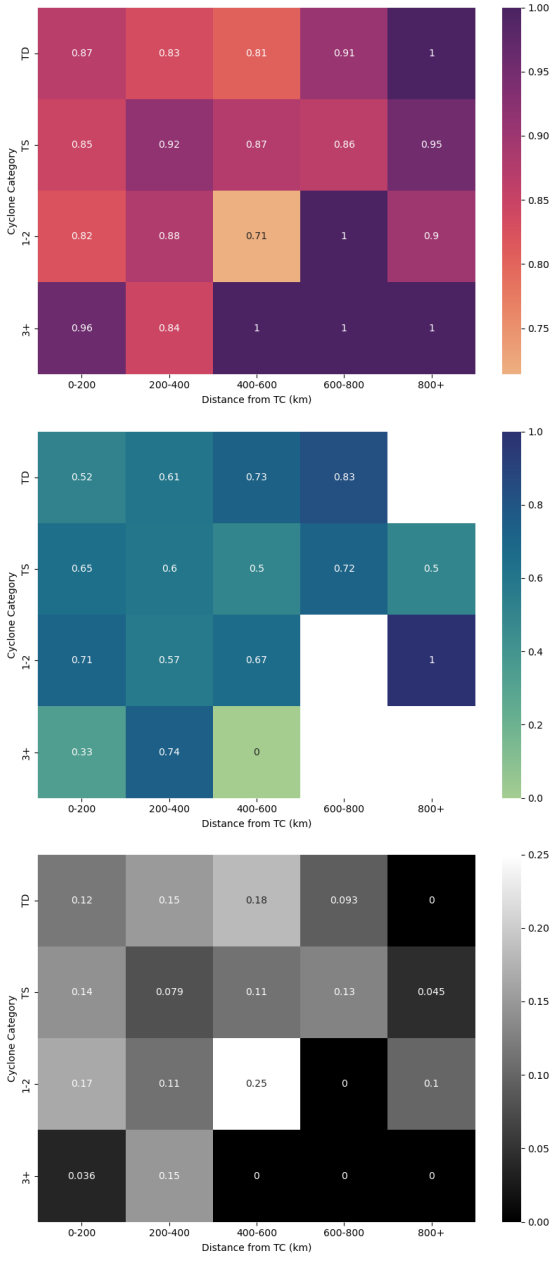

FIG. 3: Heat map showing (top) FAR, (middle) POD, and (bottom) CSI as a function of distance from TC center (km) versus TC intensity category. The annotated numbers denote the performance metric value for each cell. Note the range of the color bar differs among panels.

trades higher elevation angles for low-angle resampling, which allows for better temporal resolution of characteristics closer to the ground to compensate for the dirge of other observational data inherent with night (Chrisman 2011). This is especially critical for TC tornadic supercells

given their small horizontal and vertical scales, and rapid temporal evolution (McCaul and Weisman 1996; Edwards 2012).

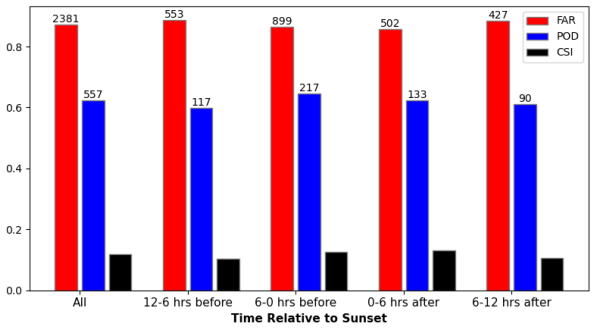

FIG. 4: As in Fig. 1, but stratified by time relative to sunset of tornado start.

c. Damage Rating

POD, perhaps intuitively, increases with damage rating as shown in Fig. 5. EF-0 tornadoes have a POD of 60.3%, EF-1 tornadoes have a POD of 63.7%, and EF2+ tornadoes have a POD of 75.9%. This is despite the majority of the strongest tornadoes forming in ranges close to the TC center (Fig. 6), where POD and CSI are slightly smaller. In conjunction with this, there is also a smaller number of weaker tornadoes, relative to EF2+ tornadoes, located near the TC center (Fig. 6). Some of this may be because confirmation of tornadoes that are not directly observed visually can be confused with damage associated with "misovortices" within the eyewall, which are believed to be generated inward of the radius of maximum wind where horizontal wind shear is large. These vortices may produce similar damage to tornadoes but differ in their dynamics (Wurman and Kosiba 2018).

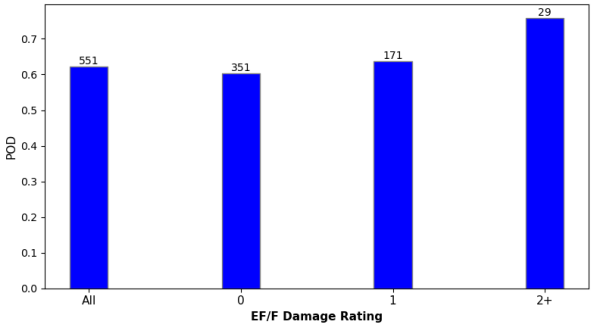

FIG. 5: Bar plot shows POD for TC tornadoes stratified by damage rating. The annotated number above each bar shows the sample size of each bin.

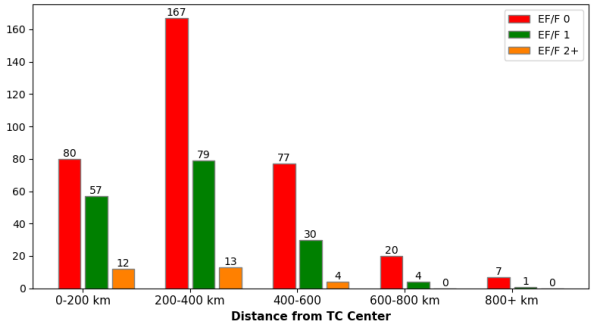

FIG. 6: Bar plot showing the distribution of tornadoes relative to TC distance from the center (km) stratified by damage rating on the EF-scale.

d. Radar Analysis

To address this, developing radar tools may be useful in establishing thresholds that operational forecasters can use to more easily compensate for observational limitations inherent to dealing with landfalling TCs. Comparison of 0.5°-tilt maximum AzShear data (Fig. 7) shows an upward shift in the distribution for warned tornadoes when compared to tornadoes which were not accurately forecast. Resampling the median of the distributions 10,000 times with replacement using a bootstrap approach revealed that the non-tornadic median was not significantly different from either the hit or missed tornadic medians at the 95% confidence interval. The median AzShear for warned tornadoes is 1.1×10^{-2} s^{-1} while the median AzShear for missed tornadoes is 7.8×10^{-3} s^{-1}, which was also found to be significantly different at p-value$<$0.05 according to a Mood's median test. In contrast, the median AzShear values for missed tornadoes and nontornadic cells were not significantly different, which reinforces the idea that nontornadic cells are difficult to distinguish from tornadic cells via radar (McCaul 1991; Devanas et al. 2008). Strong differences in extreme values for maximum AzShear are also present. Specifically, the maximum recorded value for warned tornadoes is 3.8×10^{-2} s^{-1}, while the maximums for missed and nontornadic cells are 2.6×10^{-2} s^{-1} and 2.1×10^{-2} s^{-1}, respectively.

Comparison of 0.5°-tilt minimum DivShear data (Fig. 8) was also examined. The DivShear distribution is shifted upwards for missed tornadoes when compared to warned tornadoes, though the shapes of the two distributions are qualitatively very similar. A 10,000-sample bootstrapping resampling revealed that the nontornadic median was significantly different from the hit tornadic medians, but not the missed medians at the 95% confidence interval. The median DivShear for warned tornadoes is -7.6 $\times 10^{-3}$ s^{-1} and the median DivShear for missed tornadoes is -6.0 $\times 10^{-3}$ s^{-1}, which was found to be significantly different at

p-value$<$0.05 using Mood's Median Test. Additionally, the median DivShear for warned tornadoes and nontornadic rotating cells (-6.5 $\times$ 10^{-3} s^{-1}) were found to be significantly different when tested under like constraints using a Mood's Median Test. Unlike with the AzShear distribution, the extreme values (i.e., the minimums) did not follow a discernible pattern.

Most previous studies have used V_{rot} as an evaluation of rotation, but V_{rot} sharply degrades as a function of distance from the radar, whereas AzShear and DivShear experience more marginal degradation (Mahalik et al. 2019; Sandmæl et al. 2023). AzShear and V_{rot} in particular are closely correlated with one another physically, whereas DivShear provides new information (Martinaitis 2017). Hence, AzShear and DivShear may have more value to forecasters, especially for cells that are far from the radar (Mahalik et al. 2019; Sandmæl et al. 2023).

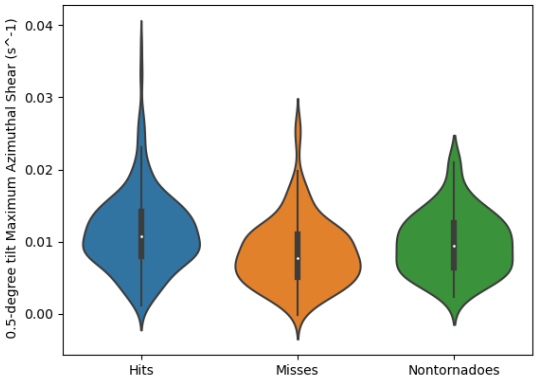

FIG. 7: Violin plot with box-and-whiskers plot overlaid showing 0.5°-tilt AzShear (s^{-1}) stratified between warned and missed tornadoes, and subjectively identified rotating supercells that were warned (i.e., false alarms).

4. Discussion and Summary

This study investigated the variability in forecasting skill and distribution for tornadoes from 43 TCs from 2011–2021. For this study, forecasting skill was defined using the statistics of FAR, POD, and CSI. Specifically, forecasting skill variability as a function of parameters such as distance from the TC center, time relative to sunset, TC intensity, and tornado damage rating was examined. Radar-derived data, AzShear and DivShear, was also used to compare tornadic supercells and nontornadic supercells, to eventually help establish warning thresholds for each to improve warning skill.

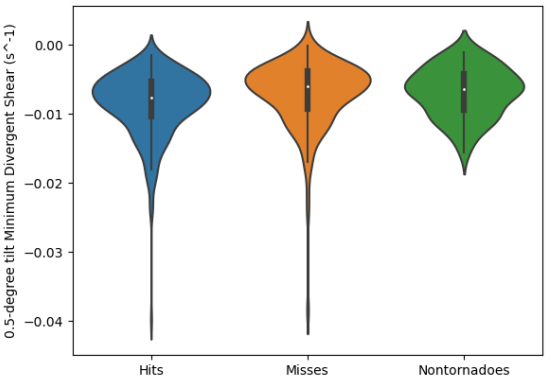

FIG. 8: As in Fig. 7, but for 0.5°-tilt DivShear (s^{-1}).

This study shows that warning skill is considerably worse for TC tornadoes than the total population of tornadoes in the United States during the period of study. Specifically, though POD is higher, so too is FAR, but to a greater extent, resulting in a significant decrease in CSI. Both warning skill and the number of tornadoes substantially decrease at distances $\geq$600 km from the TC center. Conversely, the majority of tornadoes and warnings occurred 200–400 km from the TC center, yet this bin was a local minimum in warning skill. Warning skill, and particularly FAR, were poor for strong hurricanes; this diminished warning skill extended at any distance of tornadoes from the center of strong hurricanes. Warning skill for nocturnal tornadoes was not as diminished when compared to diurnal tornadoes, which may be attributed to the adoption of modern radar scanning strategies in the study period. Overall, POD is relatively continuous throughout the day. Additionally, as damage rating increased, so did POD such that strong (EF2+) tornadoes were substantially more likely to be accurately forecast.

AzShear and DivShear may prove to be useful future tools when forecasting TC tornadoes. The medians of the maximum AzShear and minimum DivShear, respectively, differed significantly between warned and missed tornadoes. For AzShear, the extreme values differed as well, with accurately warned tornadoes associated with all the highest values.

While warning skill is worse for TC tornadoes than non-TC tornadoes forming in the continental United States, this is often a function of a much higher FAR during TCs (Martinaitis 2017; Nowotarski et al. 2021). Due to the myriad of hazards associated with landfalling TCs, warning sensitivity may be higher than for isolated supercells (Edwards 2012). This indicates that new warning strategies and instrumentation are needed for these more marginal tornado-spawning embedded cells (e.g., phased

array radar; Adachi and Mashiko 2020; Morotomi et al. 2020), some of which may be resolved using radar characteristics such as AzShear and DivShear. Tornadoes rated lower on the EF–scale tend to be harder to accurately forecast, and are an area of interest for future work, especially differentiating these tornadic cells from nontornadic, yet strongly rotating cells. Additionally, forecasters may also consider using lightning observations to aid in forecasting non-TC tornadoes, although recent work has suggested that marginal value may be added compared to radar data (Schenkel et al. 2023).

Acknowledgments. This work is generously supported by funding from NSF AGS-2050267, NSF AGS-2028151, and by the NOAA/Office of Oceanic and Atmospheric Research under the NOAA-University of Oklahoma Cooperative Agreement #NA21OAR4320204, U.S. Department of Commerce. The statements, findings, conclusions, and recommendations herein are those of the authors and do not necessarily reflect the views of OU, CIWRO, NOAA, and NSF. We would also like to extend our sincerest gratitude to Daphne LaDue (CAPS) and Alex Marmo (CAPS) for their support throughout this project.

References

Adachi, T., and W. Mashiko, 2020: High temporal-spatial resolution observation of tornadogenesis in a shallow supercell associated with Typhoon Hagibis (2019) using phased array weather radar. *Geophys. Res. Lett.*, **47**, e2020GL089 635.

Baker, A. K., M. D. Parker, and M. D. Eastin, 2009: Environmental ingredients for supercells and tornadoes within Hurricane Ivan. *Wea. Forecasting*, **24**, 223–244.

Bogner, P. B., G. M. Barnes, and J. L. Franklin, 2000: Conditional instability and shear for six hurricanes over the Atlantic Ocean. *Wea. Forecasting*, **15**, 192–207.

Brooks, H. E., 2004: Tornado-warning performance in the past and future: A perspective from signal detection theory. *Bull. Amer. Meteor. Soc.*, **85**, 837–844.

Brooks, H. E., and J. Correia Jr., 2018: Long-term performance metrics for national weather service tornado warnings. *Wea. Forecasting*, **33**, 1501–1511.

Chrisman, J., 2011: Supplemental adaptive intra-volume low-level scan (SAILS). Tech. rep., 13 pp. http://www.roc.noaa.gov/wsr88d/PublicDocs/NewTechnology/SAILS_Initial_Presentation_Sep_2011.pdf.

Devanas, A., D. Gregoria, K. Kasper, and P. Santos, 2008: Tropical cyclone induced tornadoes associated with the formation of Tropical Storm Barry. *20th Conf. on Climate Variability and Change*, New Orleans, LA, Amer. Meteor. Soc., JP.3.

Edwards, R., 2010: Tropical cyclone tornado records for the modernized National Weather Service era. *Proc., 25th Conf. on Severe Local Storms*, Denver, CO, Amer. Meteor. Soc., P3.1.

Edwards, R., 2012: Tropical cyclone tornadoes: A review of knowledge in research and prediction. *Electron. J. Severe Storms Meteor.*, **7**, 1–61.

Edwards, R., A. R. Dean, R. L. Thompson, and B. T. Smith, 2012: Convective modes for significant severe thunderstorms in the contiguous United States. Part III: Tropical cyclone tornadoes. *Wea. Forecasting*, **27**, 1507–1519.

Edwards, R., and R. M. Mosier, 2022: Over a quarter century of TCTOR: Tropical cyclone tornadoes in the WSR-88D era [Dataset]. *Proc., 30th Conf. on Severe Local Storms*, Santa Fe, NM, Amer. Meteor. Soc., 171.

Franklin, J., M. Black, and K. Valde, 2003: GPS dropwindsonde wind profiles in hurricanes and their operational implications. *Wea. Forecasting*, **18**, 32–44.

Gentry, R. C., 1983: Genesis of tornadoes associated with hurricanes. *Mon. Wea. Rev.*, **111**, 1793–1805.

Gerapetritis, H., and J. Pelissier, 2004: The critical success index and warning strategy. *17th Conference on Probablity and Statistics in the Atmospheric Sciences*, Seattle, WA, Amer. Meteor. Soc.

IEM, 2020: Iowa Environmental Mesonet (IEM) radar and warning viewer. Tech. rep. URL http://mesonet.agron.iastate.edu/GIS/apps/rview/warnings.phtml, accessed April 2019 - April 2020.

Kaplan, J., and M. DeMaria, 1995: A simple empirical model for predicting the decay of tropical cyclone winds after landfall. *J. Appl. Meteor. Climatol.*, **34**, 2499–2512.

Landsea, C. W., and J. L. Franklin, 2013: Atlantic hurricane database uncertainty and presentation of a new database format [Dataset]. *Mon. Wea. Rev.*, **141**, 3576–3592.

Mahalik, M. C., B. R. Smith, K. L. Elmore, D. M. Kingfield, K. L. Ortega, and T. M. Smith, 2019: Estimates of gradients in radar moments using a linear least squares derivative technique. *Wea. Forecasting*, **34**, 415–434.

Martinaitis, S. M., 2017: Radar observations of tornado-warned convection associated with tropical cyclones over Florida. *Wea. Forecasting*, **32**, 165–186.

McCaul, E. W., 1991: Buoyancy and shear characteristics of hurricane-tornado environments. *Mon. Wea. Rev.*, **119**, 1954–1978.

McCaul, E. W., D. E. Buechler, S. J. Goodman, and M. Cammarata, 2004: Doppler radar and lightning network observations of a severe outbreak of tropical cyclone tornadoes. *Mon. Wea. Rev.*, **132**, 1747–1763.

McCaul, E. W., and M. L. Weisman, 1996: Simulations of shallow supercell storms in landfalling hurricane environments. *Mon. Wea. Rev.*, **124**, 408–429.

Molinari, J., D. M. Romps, D. Vollaro, and L. Nguyen, 2012: CAPE in tropical cyclones. *J. Atmos. Sci.*, **69**, 2452–2463.

Molinari, J., and D. Vollaro, 2010: Distribution of helicity, CAPE, and shear in tropical cyclones. *J. Atmos. Sci.*, **67**, 274–284.

Morotomi, K., S. Shimamura, F. Kobayashi, T. Takamura, T. Takano, A. Higuchi, and H. Iwashita, 2020: Evolution of a tornado and debris ball associated with Super Typhoon Hagibis 2019 observed by x-band phased array weather radar in Japan. *Geophys. Res. Lett.*, **47**, e2020GL091 061.

NOAA National Weather Service Operations Center, 1991: NOAA Next Generation Radar (NEXRAD) level 2 base data. NOAA National Centers for Environmental Information, accessed April 2019–April 2020.

Nowotarski, C. J., J. Spotts, R. Edwards, S. Overpeck, and G. R. Woodall, 2021: Tornadoes in Hurricane Harvey. *Wea. Forecasting*, **36**, 1589–1609.

Sandmæl, T. N., and Coauthors, 2023: The tornado potential algorithm: A machine-learning probability-based tornadic circulation detection algorithm [Dataset]. *Wea. Forecasting*, **38**, 445–466.

Schenkel, B. A., K. Calhoun, T. Sandmæl, Z. Fruits, I. Schick, M. C. Ake, and B. F. Kassel, 2023: Lightning and radar characteristics of tornadoes in landfalling tropical cyclones. *J. Geophys. Res.*, accepted.

Schenkel, B. A., R. Edwards, and M. Coniglio, 2020: A climatological analysis of ambient deep-tropospheric vertical wind shear impacts upon tornadic supercells in tropical cyclones. *Wea. Forecasting*, **35**, 2033–2059.

Schneider, D., and S. Sharp, 2007: Radar signatures of tropical cyclone tornadoes in central North Carolina. *Wea. Forecasting*, **22**, 278–286.

Schultz, L. A., and D. J. Cecil, 2009: Tropical cyclone tornadoes, 1950–2007. *Mon. Wea. Rev.*, **137**, 3471–3484.

Suzuki, O., H. Niino, H. Ohno, and H. Nirasawa, 2000: Tornado-producing mini supercells associated with Typhoon 9019. *Mon. Wea. Rev.*, **128**, 1868–1882.

Wurman, J., and K. Kosiba, 2018: The role of small-scale vortices in enhancing surface winds and damage in Hurricane Harvey (2017). *Mon. Wea. Rev.*, **146**, 713–722.